Research Square

Preprints are preliminary reports that have not undergone peer review.
They should not be considered conclusive, used to inform clinical practice,
or referenced by the media as validated information.

A general, non-energetic formation route to carboxylic and fatty acids in the interstellar medium

Alfred Hopkinson

a.hopkinson@phys.au.dk

Center for Interstellar Catalysis, Aarhus University https://orcid.org/0000-0002-7849-8756

Joe Pitfield

Aarhus University https://orcid.org/0000-0002-9758-5230

Peter Saalfrank

Department of Chemistry, University of Potsdam https://orcid.org/0000-0002-5988-5945

John Thrower

Aarhus University https://orcid.org/0000-0003-0974-8077

Liv Hornekaer

Aarhus University https://orcid.org/0000-0003-0828-3642

Article

Keywords: Astrobiology, Astrochemistry

Posted Date: November 2nd, 2026

DOI: https://doi.org/10.21203/rs.3.rs-10893594/v1

License: This work is licensed under a Creative Commons Attribution 4.0 International License.
Read Full License

Additional Declarations: There is **NO** Competing Interest.

A general, non-energetic formation route to carboxylic and fatty acids in the interstellar medium

Alfred Thomas Hopkinson[1*†], Joe Pitfield[1*†], Peter Saalfrank[2], John D. Thrower[1], Liv Hornekær[1]

[1]Center for Interstellar Catalysis, Department of Physics & Astronomy, Aarhus University, 8000 Aarhus C, Denmark.
[2]Department of Chemistry, University of Potsdam, Karl-Liebknecht-Strasse 24-25, 14476 Potsdam, Germany.

*Corresponding author(s). E-mail(s): a.hopkinson@phys.au.dk; joepitfield@gmail.com;
†These authors contributed equally to this work.

Abstract

Carboxylic acids have been detected in the interstellar medium, and biologically relevant fatty acids have been identified on meteorites. However, their formation routes under interstellar conditions and possible delivery to planetary surfaces to act as molecular building blocks for the origin of life remain poorly understood. Here we demonstrate a general, non-energetic, condensed-phase formation route to carboxylic acids under astrophysical, low-temperature conditions, through the interaction of aldehydes and either O-atoms or hydroxyl radicals. This general acid formation route was investigated and confirmed experimentally through the use of infrared spectroscopy and mass spectrometry, and theoretically through the use of hybrid density functional theory and coupled cluster calculations. The finding of a non-energetic formation route from aldehydes to acids and the pathway to form biologically relevant fatty acids under interstellar conditions indicates that such molecules could form and subsequently be inherited into stellar systems, thus potentially contributing to the origin of life.

Keywords: Astrobiology, Astrochemistry

In recent years, the possible link between the origin of life on Earth and the delivery of prebiotic molecules from space has been suggested [1]. The origin and formation routes of such prebiotic molecules remain unclear. In particular, it is uncertain whether they are formed in and inherited from the interstellar medium (ISM).

Fatty acids are a group of molecules essential for known terrestrial life, being components of the building blocks of modern cell membranes [2] that separate the interior of cells from the external environment [3]. These consist of phospholipids, which are fatty acids linked to a glycerol backbone [4]. However, it is presumed that when life emerged, fatty acids, which can themselves assemble into membranes [3, 4], fulfilled this role instead [3]. Fatty acids have been detected in meteorites [5–7], indicating that this important class of molecules can be formed under extraterrestrial conditions. It has been demonstrated that simple acids such as acetic acid (CH_3COOH) [8] and biologically relevant acids such as pyruvic acid ($CH_3COCOOH$) [9] can be formed through the

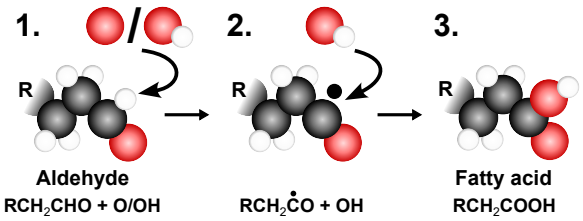


Fig. 1 The general formation route to carboxylic acids and biologically relevant fatty acids in the ISM through the exposure of aldehydes to O-atoms or $^{\bullet}$OH. 1. shows the initial stage where an aldehyde of any carbon chain length is exposed to O-atoms or $^{\bullet}$OH. This interaction leads to the abstraction of hydrogen from the formyl group and the formation of a $RCH_2C^{\bullet}O$ radical and either a $^{\bullet}$OH or water, as is depicted in 2. This radical can then react with another OH radical, which leads to the formation of a carboxylic acid group and, if the carbon chain is sufficiently long, a fatty acid, as shown in 3.

energetic processing of simple interstellar ices, and theoretical investigation has previously hypothesised excited-state $O(^1D)$ insertion as a route towards acid formation [10]. However, there is still no known route to form the larger fatty acids.

Here, we report on a combined experimental and theoretical investigation of the interactions of aldehydes with O-atoms and hydroxyl radicals ($^{\bullet}$OH) under low-temperature conditions to form acids, as shown in Figure 1. Aldehydes are a class of molecules consisting of a carbon chain terminated by a formyl group (RCHO). To date, astronomical observations have revealed the presence of nine aldehydes in the ISM, including methanal (CH_2O), ethanal (CH_3CHO) and propanal (CH_3CH_2CHO) [11, 12]. In addition, analysis of carbonaceous chondrites has also identified larger aldehydes such as butanal ($CH_3(CH_2)_2CHO$), pentanal ($CH_3(CH_2)_3CHO$) and hexanal ($CH_3(CH_2)_4CHO$) [11]. It is therefore reasonable to assume that these aldehydes also exist in the ISM.

We exposed propanal (CH_3CH_2CHO) and pentanal ($CH_3(CH_2)_3CHO$) to O-atoms in co-deposition experiments on a gold surface. The reaction for both molecules was expected to proceed via the incoming O-atom abstracting the H-atom on the formyl group, forming $^{\bullet}$OH and a propanoyl ($CH_3CH_2C^{\bullet}O$) or pentanoyl ($CH_3(CH_2)_3C^{\bullet}O$) radical respectively, which can then undergo an expectedly barrierless radical-radical recombination [13–15] with $^{\bullet}$OH to form propanoic acid (CH_3CH_2COOH) or pentanoic acid ($CH_3(CH_2)_3COOH$) as shown in Equations 1 and 2.

$$\begin{aligned} CH_3CH_2CHO + O &\rightarrow CH_3CH_2C^{\bullet}O + {}^{\bullet}OH \\ CH_3CH_2C^{\bullet}O + {}^{\bullet}OH &\rightarrow CH_3CH_2COOH \end{aligned} \quad (1)$$

$$\begin{aligned} CH_3(CH_2)_3CHO + O &\rightarrow CH_3(CH_2)_3C^{\bullet}O + {}^{\bullet}OH \\ CH_3(CH_2)_3C^{\bullet}O + {}^{\bullet}OH &\rightarrow CH_3(CH_2)_3COOH \end{aligned} \quad (2)$$

In the ISM, especially within dense molecular clouds, O-atoms are not presumed to be the main drivers of surface chemistry on dust grains and icy mantles, since they are locked up in molecules [16, 17]. Instead, ($^{\bullet}$OH), formed through reactions between oxygen and hydrogen [18–20], is hypothesized to play a key role [21, 22]. A reaction driven by $^{\bullet}$OH is considered in Equation 3 for the case of pentanal. Firstly, an $^{\bullet}$OH abstracts an H-atom, forming H_2O and the acyl radical, with recombination with a second $^{\bullet}$OH to yield the carboxylic acid.

$$\begin{aligned} CH_3(CH_2)_3CHO + {}^{\bullet}OH &\rightarrow CH_3(CH_2)_3C^{\bullet}O + H_2O \\ CH_3(CH_2)_3C^{\bullet}O + {}^{\bullet}OH &\rightarrow CH_3(CH_2)_3COOH \end{aligned} \quad (3)$$

We hypothesise that an initial aldehyde with a sufficiently long carbon chain reacts to form an acid, providing a route to the formation of biologically relevant fatty acids, such as pentanoic acid. Fatty acids could therefore be formed in the ISM, expanding the range of prebiotic molecules available in the emergence of life.

Results

Formation of propanoic acid via propanal + O-atoms

Figure 2(a,b) reveals several changes in the infrared (IR) spectrum of condensed propanal exposed to O-atoms compared to the as-deposited spectrum. The bands corresponding to the C=O stretching mode of the formyl group of propanal

at 1737 and 1695 cm^{-1} are significantly modified, with a new feature at 1720 cm^{-1}. The C=O stretching mode for propanoic acid lies in this region [23], suggesting the formation of an acid functional group. A new band between 1250 and 1186 cm^{-1}, characteristic of a C–O bond [23], supports this. Both bands are present in the reference spectrum for propanoic acid, showing good agreement with the spectrum obtained from the co-deposition of propanal and O-atoms. Band assignments of pure propanal [24, 25] and propanoic acid [23] are listed in Supplementary Table ST3 and ST4.

The spectrum of propanal exposed to O-atoms shows a sharp peak at 2350 cm^{-1}, attributed to CO_2 ice [26] originating from the O-atom source outgassing rather than from chemical reactions, as shown in Supplementary Figure SF8. The propanoic acid formed will be in a complex environment containing CO_2, water and propanal. The interactions between these species could influence the spectra, for example, the absence of the OH out-of-plane mode at 950 cm^{-1}.

The propanal + O-atom ice was annealed to 150 K, beyond the desorption point of propanal, in order to desorb any residual unreacted propanal. This resulting spectrum exhibits few propanal signatures, being dominated by bands at 1721, 1250, and 950 cm^{-1}. The spectrum shows good agreement with that obtained for propanoic acid, annealed to 150 K, with the three main bands assigned to the C=O stretching, C–O stretching, and OH out-of-plane modes, respectively, while also showing the OH stretch in the high-wavenumber region [23].

The reaction products were probed mass spectrometrically via a temperature-programmed desorption (TPD) measurement. Figure 2(c) shows the TPD traces of as-deposited propanal. The mass fragments at 57 and 58 amu correspond to propanal [27], and it can be seen to desorb from the surface at 117 K. The second desorption peak at 167 K is attributed to propanal desorbing from the sample holder, as explored in Supplementary Figure SF1. Figure 2(d) shows the TPD measurement following the co-deposition of propanal and O-atoms. Unreacted propanal can be seen, but in contrast to the as-deposited propanal TPD, the masses of propanoic acid, 45 amu, 73 amu, and 74 amu [28], are detected. These masses are in

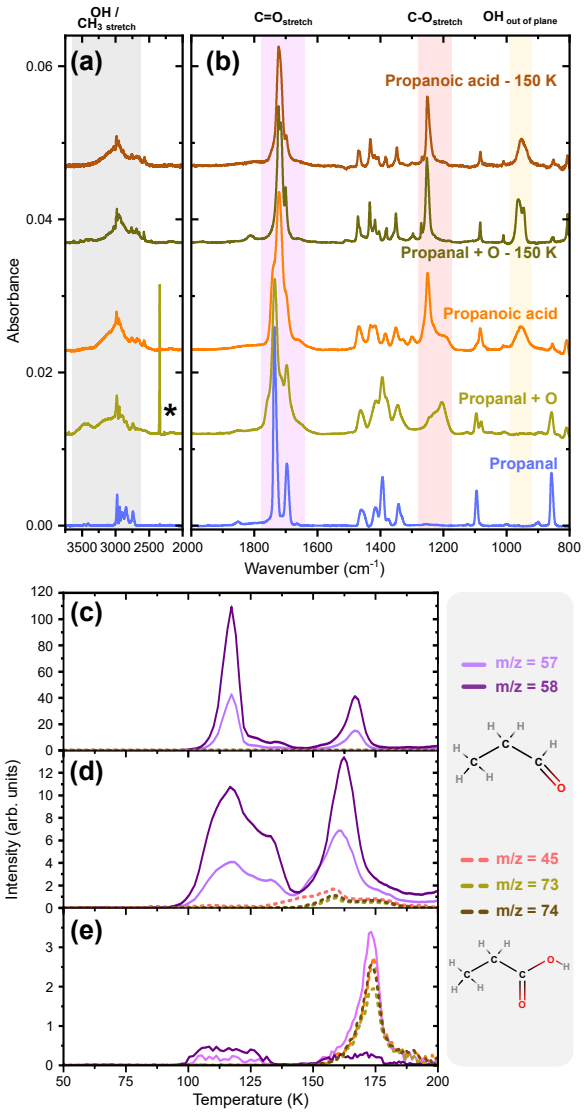


Fig. 2 FTIR spectra and TPD measurements of propanal, propanoic acid, and the measurements of propanal exposed to O-atoms. (a,b) show IR spectra of propanal (blue), propanal co-deposited with O-atoms (dark yellow), and propanoic acid (orange), all at 50 K. 50 K was used, as it is above the ozone desorption temperature and relevant for ISM conditions. Also shown are propanal exposed to O-atoms (olive) and propanoic acid (brown) annealed to 150 K. Key identifier bands have been highlighted, showing that exposure to O-atoms forms species with IR bands similar to those of propanoic acid. Marked with an * is a contamination band of CO_2 deposited from the O-atom doser. Spectra have been scaled (bottom to top) by 0.6, 1, 2, 1, and 4 for easier comparison. (c) the TPD traces of as-deposited propanal (masses 57 and 58 amu) desorbing from the sample at 117 K and a sample holder peak at 167 K. (d) TPD traces of the propanal exposed to O-atoms have characteristic propanoic acid masses (45, 73, and 74 amu) desorbing at 158 K. (e) TPD traces of the propanoic acid, desorbing at 176 K.

good agreement with the reference TPD measurement of as-deposited propanoic acid, shown in Figure 2(e), but have a broader desorption peak likely due to co-desorption with other species such as water.

Gas-phase zero-point energy (ZPE)-corrected abstraction barriers for propanal + O(^3P) (O-atom with 3 parallel spin unpaired electrons) were calculated at the CCSD(T)-F12/BHANDHLYP level to confirm the proposed reaction pathway of H-atom abstraction from the formyl group to form propanoic acid. Surface/solid-state effects are not included in this model. While the excited and highly reactive O(^1D) (O-atom with 1 unpaired electron) is known to drive reaction chemistry [29–32], these insertions exhibit much lower barriers than those of O(^3P), as shown in Supplementary Figure SF5. Reaction networks involving organic molecules and O(^1D) are thus very complex and unlikely to yield a dominant, stable reaction product. Despite having a long gas-phase lifetime, O(^1D) is highly reactive and quickly depleted. Thus, in molecular clouds with few sources capable of dissociating O_2, the relative population of O(^1D) is low, being dominated by O(^3P). We consider only the ground state O(^3P), corresponding to the study of these non-energetic reactions.

Figure 3 shows the relative energies of transition states and reaction products for the reactions of propanal and O-atoms. Reaction products occupy the singlet energy surface after spin quenching of the triplet biradical abstraction products. TS_1, shown in Supplementary Table ST2, involves the abstraction of the hydrogen from the formyl carbon, with a negligible energy barrier of 0.028 eV. This abstraction forms the $CH_3CH_2C^{\bullet}O$ radical in a spin-correlated radical pair with $^{\bullet}OH$. Upon loss of correlation through spin relaxation, this pair recombines to form the particularly stable product, propanoic acid. We attribute this low activation energy to the strong localisation of electronegativity at the carbon-oxygen double bond, weakening the covalent attraction between the formyl carbon and hydrogen.

Abstraction of an H-atom from the α-carbon (TS_2) follows two possible channels, split slightly from energetic degeneracy by symmetry breaking due to the presence of the formyl group. Both channels, however, exhibit barriers of around 0.3 eV. The radical-radical recombination products

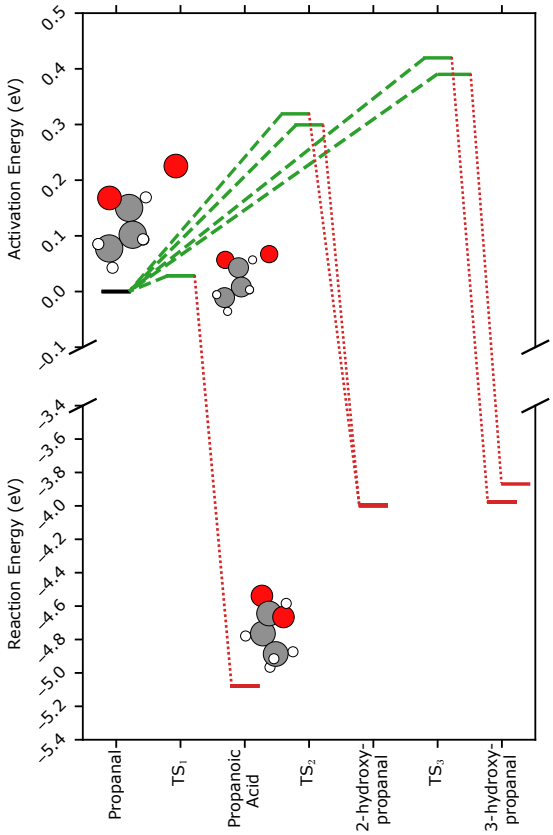


Fig. 3 Shown are the ZPE-corrected CCSD(T)-F12/BHANDHLYP level transition state energies and products for reactions of O-atoms with propanal. In green are the transition state energies for several possible hydrogen abstraction reactions, labelled TS_1, TS_2, and TS_3 respectively, indicating the carbon to which the abstracted hydrogen is initially bonded. Each transition state energy is relative to that of the pre-reaction complex. Reaction coordinates with multiple lines corresponding to reactions on the same carbon indicate stereoisomerically unique sites. The corresponding geometries of these transition states can be found in Supplementary Table ST2. In red, three proposed radical-radical recombination products proceeding from hydrogen abstraction, where extra lines indicate the presence of higher-energy metastable conformers or stereoisomers. The pathway with the lowest barrier, $CH_3CH_2CHO + O \rightarrow CH_3CH_2C^{\bullet}O + OH \rightarrow CH_3CH_2COOH$, is accompanied by molecular illustrations. The energy of each of the pre-reaction complexes is shifted to 0 eV, such that the barrier heights can be directly compared. Green lines indicate the highest point along the minimum energy pathway connecting the pre-reaction complex with the post-reaction products. Red lines indicate the energy of the resulting product after radical-radical recombination.

for this reaction pathway are more energetically degenerate than the transition states, indicating a weak thermodynamic impact of the functional group. A further three hydrogen abstraction channels are possible from the terminal carbon. The classical barriers for the abstraction of either of the two enantiotopic hydrogens are functionally degenerate (0.42 eV), indicating that the interaction with the formyl group is weak. The inequivalent hydrogen has a slightly lower energy barrier (0.39 eV). Regardless, the transition state energies are substantially higher than those of the formyl hydrogen. In addition, for reactions involving each of the 5 non-formyl hydrogens, the products are significantly less exothermic.

Previous studies [33] indicate that tunnelling plays an important role in the abstraction of H-atoms. While tunnelling may allow access to TS_2 and TS_3 channels, the similar geometry of transition states of all considered channels is sufficient to posit that the much lower barrier of TS_1 will result in that reaction pathway dominating. We consider the possibility that O-atoms could react further with propanoic acid, as shown in Supplementary Figure SF2. This revealed uniformly high activation energies, leading to the conclusion that there are no further reactions.

Both the presented experimental and theoretical results indicate that O-atom reactions with propanal predominantly yield propanoic acid, with the reaction having both the lowest energy barrier and being the most energetically favourable product. To assess the generality of this formation route and its potential role in forming biologically relevant fatty acids, we extend the study to a longer carbon chain aldehyde.

Formation of pentanoic acid via pentanal + O-atoms

Figure 4(a,b) shows the IR spectra of pentanal exposed to O-atoms. Compared to the as-deposited spectrum, several differences can be observed, notably the C=O stretching mode of the formyl group at 1720 cm^{-1} becoming broadened. This is consistent with the formation of an acid functional group, exhibiting a broad absorbance feature centred at 1717 cm^{-1}. At 1205 cm^{-1}, a new band attributed to the C–O stretching mode of the acid group can be seen. A broad band around 3000 cm^{-1} in Figure 4(a) is present, likely a O–H stretching mode arising from a combination of both H_2O outgassed from the oxygen source and from the acid group of pentanoic acid. After annealing to temperatures above the desorption temperature of pentanal, the co-deposited ice and reference pentanoic acid ice closely match, supporting pentanoic acid formation.

Figure 4(c) shows TPD traces 57 and 58 amu [34] for as-deposited pentanal desorbing from the sample at 135 K. A smaller desorption peak at 185 K is attributed to pentanal desorption from the sample holder. Figure 4(d) shows TPD traces for pentanal co-deposited with O-atoms, revealing a new desorption peak at 188 K of masses 60 and 73 amu. Both the masses [35] and desorption temperature match those of pure pentanoic acid, presented in Figure 4(e), strongly indicating pentanoic acid formation. There are signatures for masses 57 and 58 amu, which we attribute to the desorption of unreacted pentanal bound to the acid and desorption from the sample holder.

To test that this reaction also occurs for a film of aldehyde exposed to O-atoms, pentanal was first deposited and subsequently exposed. The IR and TPD measurements are shown in Supplementary Figure SF6 and likewise show pentanoic acid formation. The co-deposition experiment was also repeated on a highly oriented pyrolytic graphite surface. As shown in Supplementary Figure SF7, pentanoic acid formation was also observed, demonstrating that the gold substrate had no catalytic effect.

The activation energies for reactions of $O(^3P)$ with pentanal were calculated as for propanal. Figure 5 shows the possible hydrogen abstraction reactions upon $O(^3P)$. TS_1, centralised for clarity, lies along the pathway to pentanoic acid and exhibits both the lowest activation energy and the most stable product. The activation barrier for the abstraction of the H-atom from the formyl group (0.030 eV) is comparable to that for propanal (0.028 eV). This indicates that the carbon chain length does not strongly influence this reaction and that abstraction of the H-atom from the formyl group by an O-atom is favourable, thus expected to be the dominant reaction pathway.

Reactions of an O-atom with the second and third carbons, TS_2 and TS_3 proceed with barriers comparable to those for the α-carbon of propanal, with very similar barriers for $TS_{2,1}$ and

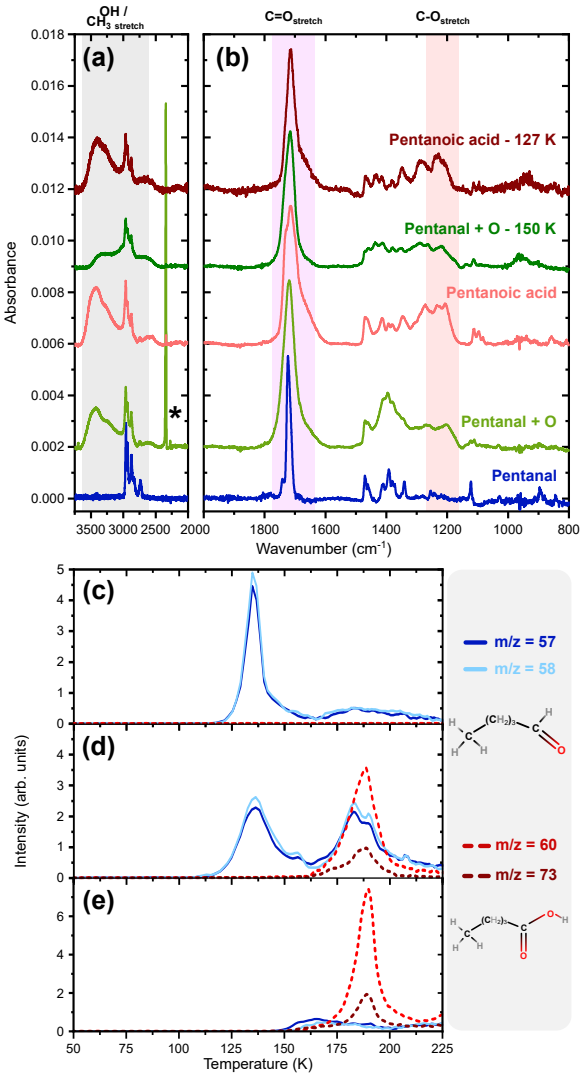


Fig. 4 FTIR spectra and TPD measurements of pentanal, pentanoic acid, and the measurements of pentanal exposed to O-atoms. (a,b) show IR spectra of pentanal (dark blue), pentanal co-deposited with O-atoms (light green), and pentanoic acid (salmon), all at the base temperature of 50 K. Also shown is pentanal exposed to O-atoms (dark green), annealed to 150 K, and pentanoic acid measured during a TPD measurement at 127 K. Key identifier bands have been highlighted, showing that pentanal exposed to O-atoms forms species with IR bands that match those of pentanoic acid. Marked with an * is a contamination band of CO_2 deposited from the atom doser. (c) TPD traces for as-deposited pentanal (masses 57 and 58 amu), with its desorption peak at 135 K and a sample holder peak at 185 K. (d) TPD traces for pentanal co-deposited with O-atoms revealing the characteristic propanoic acid fragment masses (60 and 73 amu) desorbing at 188 K. (e) as-deposited pentanoic acid with its desorption peak centred at 190 K.

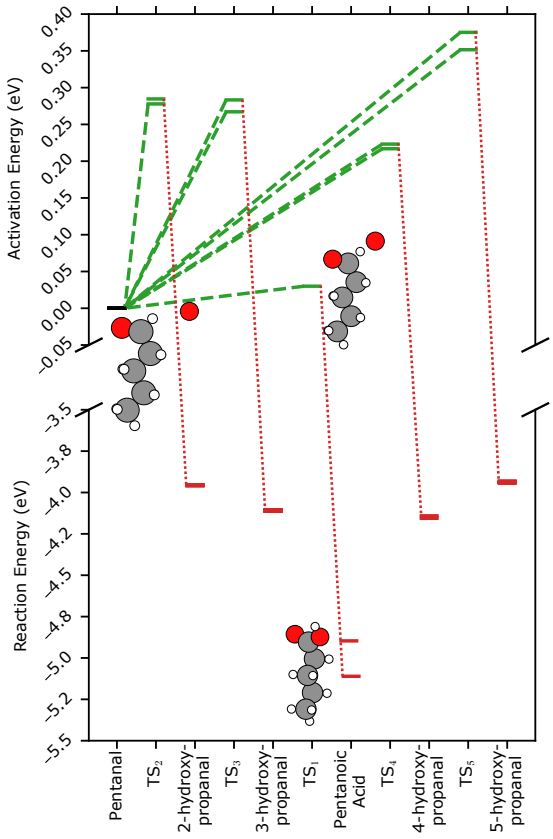


Fig. 5 ZPE-corrected CCSD(T)-F12/BHANDHLYP level transition state energies of H-atom abstraction reactions upon O-atom impingement on pentanal. They are labelled TS_1, TS_2, TS_3, TS_4 and TS_5, highlighted in green, where the indices indicate the carbon to which the abstracted hydrogen is initially bonded. The pathways with multiple lines corresponding to the same carbon atom indicate stereoisomerically unique sites. The corresponding geometries of these transition states can be found in Supplementary Table ST2. Five proposed radical-radical recombination products that can be formed following H-atom abstraction are highlighted in red, where extra lines indicate the presence of higher-energy metastable conformers or stereoisomers. The pathway with the lowest barrier, $CH_3(CH_2)_3CHO + O \rightarrow CH_3(CH_2)_3C^{\bullet}O + OH \rightarrow CH_3(CH_2)_3COOH$, is accompanied by molecular illustrations.

$TS_{2,2}$. Reactions at the penultimate carbon atom (TS_4) have noticeably smaller activation energies, with a similar increase in thermodynamic stability of the products. In this case, the transition states and products obtained through abstraction of the two possible H-atoms are almost degenerate in energy. Abstractions $TS_{5,2}$ and $TS_{5,3}$ from the terminal carbon yield degeneracy between the

two enantiotopic H-atoms, as seen for propanal. Abstraction $T5_{5,1}$ has a slightly higher activation energy, although all three products have similar thermodynamic stability. From a kinetic and thermodynamic viewpoint, TS_5 is the least viable.

The possibility of further reactions of pentanoic acid when exposed to O-atoms was considered, as shown in Supplementary Figure SF3. Whilst activation energies differ when compared to the corresponding sites for pentanal, there is no indication that acid formation has enabled further low-temperature O(^3P) reactions.

These results demonstrate that the formation of the carboxylic acid through abstraction of the H-atom on the formyl group and subsequent recombination with $^\bullet$OH is the dominant reaction channel. This could provide a general formation route to both simple carboxylic acids and biologically relevant fatty acids under ISM conditions.

Reactions involving hydroxyl radicals

Pentanal and propanal were exposed to $^\bullet$OH via co-deposition with O-atoms and H-atoms. H- and O-atoms react together to form water with several intermediate steps involving or producing $^\bullet$OH [36]. To ensure that O-atoms were not responsible for the majority of the reactions, the hydrogen dosing flux was in excess by using an H_2 feed pressure six times that used for O_2. The results are shown in Figure 6, with IR measurements for both propanal and pentanal, a TPD for pentanal, and theoretical calculations for pentanal.

Figure 6(a,b) reveal several IR bands associated with the formation of propanoic acid and pentanoic acid, respectively. At 1715 cm^{-1} is the band associated with the C=O stretching mode of the acid group, with the C–O stretching mode present at 1231 cm^{-1}. The presence of the O–H stretching mode from the acid group around 3000 cm^{-1} cannot be identified clearly due to a strong broad absorbance centred at 3385 cm^{-1}, which is attributed to the $^\bullet$OH stretching mode of water [37]. This is consistent with the formation of H_2O when co-depositing O- and H-atoms, demonstrated in Supplementary Figure SF8.

In Figure 6(c), the traces for the characteristic fragment masses of pentanal (57 and 58 amu) [34] and pentanoic acid (60 and 73 amu) [35] are plotted. The detection of the characteristic pentanoic acid masses at 192 K supports the conclusion that the reaction between $^\bullet$OH and pentanal forms pentanoic acid.

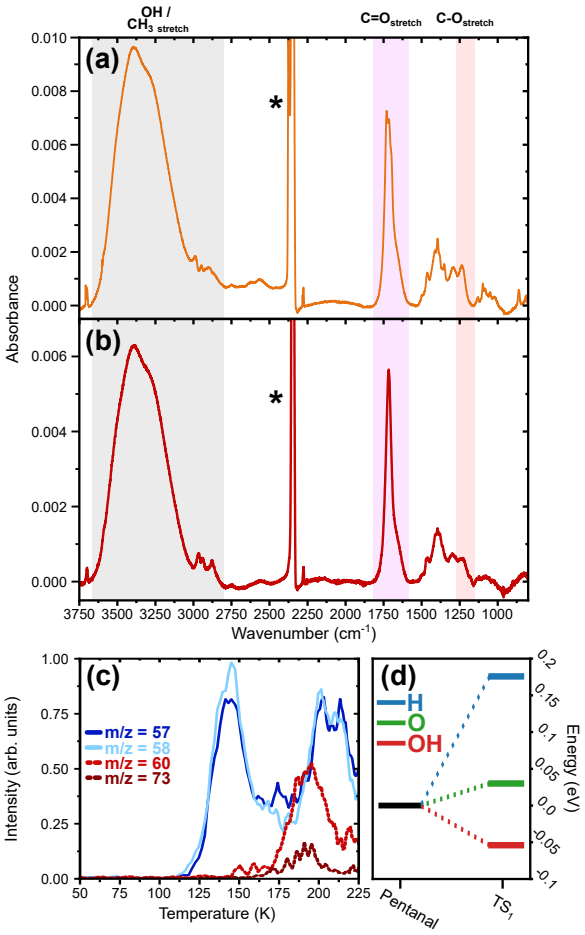


Fig. 6 IR spectrum of propanal and pentanal, TPD traces corresponding to pentanal, all having been exposed to $^\bullet$OH, and the theoretically calculated energy barriers for abstracting hydrogen from the formyl group with different species. (a) shows the IR spectrum of propanal co-dosed with H and O-atoms to process it with $^\bullet$OH, and (b) shows the same for pentanal. The spectra have the main bands highlighted, showing indications of acid formation. Marked with an * is a contamination band of CO_2 deposited from the atom doser. (c) shows the TPD measurement of the same experiment. Pentanal (masses 57 and 58 amu) desorbs first, followed by pentanoic acid (masses 60 and 73 amu). (d) shows the ZPE-corrected barrier heights of the transition states of the pentanal TS_1 for three reactants, H-atoms, O-atoms and $^\bullet$OH.

The first step in the O-atom reactions is the abstraction of the H-atom from the formyl group,

forming an acyl radical. It is therefore interesting to compare the relative abstraction energies for O- and H-atoms, as well as $^{\bullet}$OH. Figure 6(d) compares the ZPE-corrected barrier heights of the relevant transition states, TS_1., associated with each of these species with respect to the pre-reaction complexes of their respective reactants.

The barriers for both O-atoms and $^{\bullet}$OH are small compared to those for the other sites in Figures 3 and 5, while abstraction by an H-atom has the highest barrier at almost 0.2 eV. Both O-atoms and $^{\bullet}$OH demonstrate low barriers, with the $^{\bullet}$OH vibrationally adiabatic barrier sitting slightly below the pre-reactive complex in terms of energy. This artefact arises from the flat nature of the local potential energy surface and the structural similarity between the early DFT transition state and the van der Waals complex. Energetically, this indicates that the system faces no internal thermodynamic barrier upon entering the reaction well, rendering the hydrogen abstraction an effectively barrierless process from the pre-reactive complex, followed by radical-radical recombination to form acids, which overall suggests that this route is important even at low temperatures.

Discussion

Although fatty acids have not yet been detected within the ISM, observations have revealed shorter carbon-chain carboxylic acids such as formic acid (HCOOH) [12, 38] and acetic acid (CH_3COOH) [12, 39]. Fatty acids have been found on meteorites [5–7], highlighting the possibility that they could have been formed in, and be inherited from, the ISM. Simple aldehydes have been identified in the ISM through observations, such as propanal [11, 12], and larger aldehydes have been detected on carbonaceous chondrites, such as pentanal [11]. The present work indicates that reactions involving aldehydes can provide a low-temperature route to the formation of both simple carboxylic and longer-chain fatty acids under ISM conditions.

The reactions explored in this work could provide a route to carboxylic acid formation throughout most of the lifetime of an interstellar cloud. Specifically, through exposure of aldehydes to both O-atoms and $^{\bullet}$OH. In the ISM, O-atoms exist primarily during the early stages of cloud formation, before being locked up in molecules [16, 17]. The reaction route involving O-atoms is therefore most relevant earlier in a cloud's lifetime, assuming aldehydes are present. $^{\bullet}$OH are more likely drivers of acid formation during the later stages of cloud evolution in the ISM where it can be formed on the surfaces of dust grains through reactions between H- and O-atoms [18–20], and also through the energetic processing of water ice sources such as UV or cosmic rays [40, 41]. However, irradiation of ices containing organic molecules can lead to the production of highly reactive species, including $O(^1D)$ [42], which does not lead to such convergent reaction pathways. Thus, while the necessary drivers for the proposed route to acid formation are present throughout the lifetime of an interstellar cloud, we suggest that non-energetic processes dominate the formation of interstellar fatty acids.

The proposed reaction pathway can be considered a general route to acid formation, requiring only the presence of an aldehyde functional group on a molecule. This means that, regardless of the chain length, exposure of an aldehyde to O-atoms or $^{\bullet}$OH can lead to carboxylic acid formation via formyl group attack. It is therefore likely that fatty acids of a range of chain lengths, including branched chains, could be formed. This would significantly increase the chemical complexity of complex organic molecules (COMs) in the ISM and may lead not only to the formation of fatty acids, but also to reactions with other molecules that have formyl groups. For example, large biologically relevant COMs, such as peptides formed through atomic carbon condensation, are terminated with a formyl group [43]. The reaction presented in this paper could therefore be a possible pathway to create an acid and a more biologically relevant peptide.

The formation of fatty acids of differing sizes in the ISM could result in these biologically relevant molecules being available to be inherited into stellar bodies during cloud collapse. They may survive this process and be inherited into planetary bodies such as meteorites and comets that can then deliver these molecules to planetary surfaces to be involved in the origin of life.

Methods

Experimental

Experiments were carried out using an ultra-high vacuum (UHV) chamber in the Surface

Dynamics Laboratory (SDL) at the Department of Physics & Astronomy at Aarhus University. The chamber had a base pressure of ca. 10^{-10} mbar. Reflection absorption infrared spectroscopy (RAIRS) measurements were performed with a Bruker Vertex 80v FTIR spectrometer coupled to the UHV chamber. Incident IR radiation was directed via an off-axis parabolic mirror onto an optically polished, gold-plated copper substrate at the centre of the chamber at an incidence angle of 82°. The reflected light was refocused onto a liquid nitrogen-cooled mercury-cadmium-telluride (MCT) detector (Infrared Associates). The FTIR spectrometer and housings for the guiding optics and MCT detector were isolated from the UHV chamber by means of IR-transparent KBr windows, and evacuated to <3 mbar with a scroll pump. The gold-plated substrate was mounted on the end of a copper cold finger cooled by a closed-cycle helium cryostat (Sumitomo Cryogenics RDK-408E) to a base temperature of ca. 17 K as measured with a K-type thermocouple previously calibrated using a silicon diode attached to the same position. The sample could be heated to ca. 300 K with the aid of a cartridge heater (Lakeshore Cryotronics HTR-25-100) controlled by a cryogenic PID controller (Lakeshore Cryotronics Model 336). Both atom and molecule deposition, as well as temperature-programmed desorption (TPD) measurements, could be performed without moving the sample from the optimal RAIRS position.

TPD measurements were performed with a quadrupole mass spectrometer (QMS; Pfeiffer Vacuum HiQuad QMG700) with a mass range of 1-2048 amu, with its axis along the normal to the sample. Molecular species were introduced via a fine leak valve through a stainless steel tube directed at the sample, terminating ca. 40 mm from the centre of the chamber. Atomic beam sources for oxygen (MBE Komponenten GmbH OBS) and hydrogen (MBE Komponenten GmbH HABS). Both sources produce an atomic beam by passing the precursor species through a hot capillary (W and Ir for H_2 and O_2, respectively. Both atomic beams were incident at an incidence angle of 30°.

The liquid samples were prepared on a dedicated high-vacuum gas-handling manifold with a base pressure of $< 5 \times 10^{-9}$ mbar, each being purified through multiple freeze-pump-thaw cycles. All deposited molecules were purchased from TCI. Propanal had > 98% purity, pentanal had > 95% purity, propanoic acid had > 99% purity, and pentanoic acid had > 98% purity.

For the atomic beam sources, the supply lines were flushed several times prior to filling with O_2(Praxair 99.999%) and H_2 (Praxair 99.999%). The gas feed pressures were regulated by independent fine leak valves and measured with a Pirani gauge.

Prior to each measurement, the substrate was annealed to 300 K to remove any adsorbed contaminants before being cooled back to base temperature. Prior to deposition, a background RAIR spectrum in the range (5000-750 cm^{-1}) was obtained through the co-addition of 1024 scans with a spectral resolution of 1 cm^{-1}. The target molecule was then introduced into the chamber through the fine leak valve, with the chamber pressure measured by a hot cathode ionisation gauge (Vacgen ZVIG18). For co-depositions, either the OBS or both the OBS and HABS were operated simultaneously during the molecular deposition for the oxygen and $^{\bullet}$OH measurements, respectively. For the layered systems discussed in the Supplementary Information, the relevant atomic sources were operated after the molecular deposition.

The temperature of the beams was ca. 2000 K, and the $^{\bullet}$OH that was formed through interactions of H-atoms and O-atoms on the surface and is therefore assumed to have thermalised. The atomic fluxes of the HABS and OBS are dependent on the geometry of the source, feed pressure and temperature of the source [44]. Both sources have a nominal atomic flux of the order of 10^{14} $cm^{-2}s^{-1}$. The feed pressure used for the HABS was six times greater than that for the OBS in order to have an excess of hydrogen atoms.

Repeated RAIR spectra were obtained during depositions, and the masses of key fragment ions were monitored simultaneously to assess the purity. Once the deposition was complete, a final RAIR spectrum was obtained through the co-addition of 1024 scans. The TPD measurement was then performed with a linear ramp of 30 K/s, split into several steps if needed. The reason for being split into two was to enable changes in the IR spectra to be observed due to molecules desorbing. IR measurements taken during TPD measurements consist of 64 coadded scans.

Theoretical

The theoretical calculations were performed through the Center for Scientific Computing at Aarhus University (CSCAA). Two levels of *ab initio* theory have been applied across this work. For the determination of equilibrium and transition state structures, as well as the calculation of thermodynamic properties such as ZPE energy corrections, a GGA hybrid functional DFT approach was applied. We selected the BHANDHLYP/def2-TZVP functional/basis set. The functional consists of a mixture of 50% of Becke's [45] three-parameter exchange functional and 50% exact Hartree-Fock exchange. The Lee-Yang-Parr correlation functional [46] accounts for electron correlation. This functional was found to describe hydrogen abstraction reaction geometries well in other works [47–51]. The B3LYP (20% HF) functional was, conversely, unable to accomplish the task of obtaining transition states for a majority of reactions considered herein. In addition to this functional, the D4 correction of Grimme [52] was applied to account for long-range dynamic correlation effects.

All classical energy barriers presented were obtained with respect to the total energy of the pre-reaction complex. Pre-reaction complexes and reaction product geometries and energies were obtained through hybrid DFT structural relaxation using the BFGS algorithm as implemented in the Atomic Simulation Environment (ASE) [53] software package, to a low force convergence criteria of 0.01 eV/Å. Transition state geometries were obtained through nudged elastic band calculations, using the FIRE optimiser and performed as implemented in ASE, with a force convergence criteria of 0.025 eV/Å, utilising IDPP [54] interpolation to generate initial images, and 20 images along the band unless otherwise required, wherein up to thirty images were used in the event of numerical instability. The climbing image convention was applied to converge towards the final transition state. Transition states are verified by the existence of a single imaginary mode.

Reaction barrier energies were subsequently refined with single-point energy calculations at the CCSD(T)-F12 level using the cc-pVDZ-F12 basis set with cc-pVDZ-F12-CABS and cc-pVTZ/C auxiliary basis sets, as implemented in ORCA [55]. Reactant, TS, and product energies were corrected with ZPE energies calculated with BHANDHLYP/def2-TZVP as implemented in ORCA. These corrections are obtained from frequencies calculated under harmonic approximation. All ZPE corrected classical barriers are reported as vibrationally adiabatic barriers at 0 K. The resulting procedure is referred to as CCSD(T)-F12/BHANDHLYP throughout. Oxygen atoms were considered to occupy the $O(^3P)$ energy surface throughout hydrogen abstraction, which has been shown to occur on the triplet energy surface for related molecules [56]. Products are assumed to form on the singlet energy surfacer after quenching of spin-correlated biradical triplets. Strictly, a fully quantitative approach would require analysis of intersystem crossing during abstraction. However, as this process is governed by spin-orbit coupling and we exclusively consider light elements, any impact is expected to be small.

A benchmark of this approach has been performed for hydrogen abstraction from methane, and the results have been compared to previously obtained values, see SF4. We find good agreement with the barriers obtained in the literature with this method.

Data Availability

Data for this project will be available via Zenodo.

Acknowledgments

Support from the Danish National Research Foundation through the Centre of Excellence 'InterCat' (grant agreement No. DNRF150) is acknowledged. The research was supported by the European Union, under ERC Synergy Grant 101163161, 'IRASTRO', 'Molecular quantum dynamics in low temperature condensed phase astrochemistry'.

Fruitful discussions with Elham Mazarei are gratefully acknowledged.

Author contributions statement

A.T.H. and J.P. devised the investigation. A.T.H. conducted the experimental investigation with input from J.D.T. J.P. conducted the theoretical

calculations with input from P.S. A.T.H. and J.P. analysed the results with input from J.D.T., P.S., and L.H. A.T.H., J.P., J.D.T., and L.H. wrote the manuscript. All authors read and approved the paper.

Competing interests statement

There are no known competing interests.

References

[1] Chatterjee, S. *Origin of Life: A Model of Hierarchical Complexity*, 21–29 (Springer International Publishing, Cham, 2023). URL https://doi.org/10.1007/978-3-031-23397-5_4.

[2] De Carvalho, C. C. C. R. & Caramujo, M. J. The various roles of fatty acids. *Molecules* **23** (2018). URL https://www.mdpi.com/1420-3049/23/10/2583.

[3] Cho, C. J. *et al.* Protocells by spontaneous reaction of cysteine with short-chain thioesters. *Nature chemistry* **17**, 148–155 (2025).

[4] Cohen, Z. R. *et al.* Plausible sources of membrane-forming fatty acids on the early earth: A review of the literature and an estimation of amounts. *ACS Earth and Space Chemistry* **7**, 11–27 (2023). URL https://doi.org/10.1021/acsearthspacechem.2c00168.

[5] Lai, J. C.-Y., Pearce, B. K., Pudritz, R. E. & Lee, D. Meteoritic abundances of fatty acids and potential reaction pathways in planetesimals. *Icarus* **319**, 685–700 (2019). URL https://www.sciencedirect.com/science/article/pii/S0019103518304172.

[6] Lai, J. C.-Y., Pearce, B. K., Pudritz, R. E. & Lee, D. Meteoritic abundances of fatty acids and potential reaction pathways in planetesimals. *Icarus* **319**, 685–700 (2019). URL https://www.sciencedirect.com/science/article/pii/S0019103518304172.

[7] Yuen, G. U. & Kvenvolden, K. A. Monocarboxylic acids in murray and murchison carbonaceous meteorites. *Nature* **246**, 301–303 (1973).

[8] Kleimeier, N. F., Eckhardt, A. K. & Kaiser, R. I. A mechanistic study on the formation of acetic acid (ch3cooh) in polar interstellar analog ices exploiting photoionization reflectron time-of-flight mass spectrometry. *The Astrophysical Journal* **901**, 84 (2020). URL https://doi.org/10.3847/1538-4357/abafa4.

[9] Kleimeier, N. F., Eckhardt, A. K., Schreiner, P. R. & Kaiser, R. I. Interstellar formation of biorelevant pyruvic acid (ch3cocooh). *Chem* **6**, 3385–3395 (2020). URL https://www.sciencedirect.com/science/article/pii/S2451929420305246.

[10] Bates, D., Esselman, B. J., Schultz, C. P. & Widicus Weaver, S. L. Theoretical investigation of the reaction of o(1d) with formamide. *The Journal of Physical Chemistry A* **128**, 9426–9432 (2024). URL https://doi.org/10.1021/acs.jpca.4c05611.

[11] Wang, J. *et al.* Interstellar formation of lactaldehyde, a key intermediate in the methylglyoxal pathway. *Nature Communications* **15** (2024).

[12] McGuire, B. A. 2021 census of interstellar, circumstellar, extragalactic, protoplanetary disk, and exoplanetary molecules. *The Astrophysical Journal Supplement Series* **259**, 30 (2022). URL https://doi.org/10.3847/1538-4365/ac2a48.

[13] Tao, Y., Jasper, A. W., Georgievskii, Y., Klippenstein, S. J. & Sivaramakrishnan, R. Termolecular chemistry facilitated by radical-radical recombinations and its impact on flame speed predictions. *Proceedings of the Combustion Institute* **38**, 515–522 (2021). URL https://www.sciencedirect.com/science/article/pii/S1540748920304351.

[14] Butscher, T., Duvernay, F., Rimola, A., Segado-Centellas, M. & Chiavassa, T. Radical recombination in interstellar ices, a not so simple mechanism. *Physical Chemistry Chemical Physics* **19**, 2857–2866 (2017). URL https://doi.org/10.1039/c6cp07024h.

[15] Piletic, I. R., Edney, E. O. & Bartolotti, L. J. Barrierless reactions with loose transition states govern the yields and lifetimes of organic nitrates derived from isoprene. *The Journal of Physical Chemistry A* **121**, 8306–8321 (2017). URL https://doi.org/10.1021/acs.jpca.7b08229.

[16] Whittet, D. C. B. Oxygen depletion in the interstellar medium: Implications for grain models and the distribution of elemental oxygen. *The Astrophysical Journal* **710**, 1009 (2010). URL https://doi.org/10.1088/0004-637X/710/2/1009.

[17] Wang, S., Li, A. & Jiang, B. W. The interstellar oxygen crisis, or where have all the oxygen atoms gone? *Monthly Notices of the Royal Astronomical Society* **454**, 569–575 (2015). URL https://doi.org/10.1093/mnras/stv1900.

[18] Molpeceres, G. *et al.* Silicate-mediated interstellar water formation: a theoretical study. *Monthly Notices of the Royal Astronomical Society* **482**, 5389–5400 (2019). URL https://doi.org/10.1093/mnras/sty3024.

[19] Ioppolo, S., Cuppen, H. M., Romanzin, C., van Dishoeck, E. F. & Linnartz, H. Laboratory evidence for efficient water formation in interstellar ices. *The Astrophysical Journal* **686**, 1474 (2008). URL https://doi.org/10.1086/591506.

[20] Dulieu, F. *et al.* Experimental evidence for water formation on interstellar dust grains by hydrogen and oxygen atoms. *Astronomy and Astrophysics* **512**, A30 (2010). URL https://doi.org/10.1051/0004-6361/200912079.

[21] Sameera, W. M. C. *et al.* Modelling the radical chemistry on ice surfaces: An integrated quantum chemical and experimental approach. *Frontiers in Astronomy and Space Sciences* **Volume 9 - 2022** (2022). URL https://www.frontiersin.org/journals/astronomy-and-space-sciences/articles/10.3389/fspas.2022.890161.

[22] Tsuge, M. & Watanabe, N. Behavior of hydroxyl radicals on water ice at low temperatures. *Accounts of Chemical Research* **54**, 471–480 (2021).

[23] Jakobsen, R., Mikawa, Y., Allkins, J. & Carlson, G. The vibrational spectra of propanoic acid. *Journal of Molecular Structure* **10**, 300–303 (1971). URL https://www.sciencedirect.com/science/article/pii/0022286071870898.

[24] Yarnall, Y. Y., Gerakines, P. A. & Hudson, R. L. Propanal, an interstellar aldehyde - first infrared band strengths and other properties of the amorphous and crystalline forms. *mnras* **494**, 4606–4615 (2020).

[25] Qasim, D. *et al.* Formation of interstellar propanal and 1-propanol ice: a pathway involving solid-state CO hydrogenation. *aap* **627**, A1 (2019).

[26] Suhasaria, T., Leuschner, V., Jäger, C., Gieser, C. & Henning, T. Co2 infrared spectra on silicate dust grain analogs: Implications for jwst observations. *The Astrophysical Journal Letters* **988**, L27 (2025). URL https://doi.org/10.3847/2041-8213/ade993.

[27] NIST Mass Spectrometry Data Center. Propanal (2025). URL https://webbook.nist.gov/cgi/cbook.cgi?ID=C123386&Mask=200#Mass-Spec.

[28] NIST Mass Spectrometry Data Center. Propanoic acid (2025). URL https://webbook.nist.gov/cgi/cbook.cgi?ID=C79094&Mask=200#Mass-Spec.

[29] Carder, J. T., Ochs, W. & Herbst, E. Modelling the insertion of o(1d) into methane on the surface of interstellar ice mantles. *Monthly Notices of the Royal Astronomical Society* **508**, 1526–1532 (2021). URL https://doi.org/10.1093/mnras/stab2619.

[30] Hickson, K. M. & Loison, J.-C. Kinetic study of the gas-phase o(1d) + ch3oh and o(1d) + ch3cn reactions: Low-temperature rate constants and atomic hydrogen product yields. *The Journal of Physical Chemistry A* **126**, 3903–3913 (2022). PMID: 35687018.

[31] Bates, D., Esselman, B. J., Schultz, C. P. & Widicus Weaver, S. L. Theoretical investigation of the reaction of o(1d) with formamide. *The Journal of Physical Chemistry A* **128**, 9426–9432 (2024). URL https://doi.org/10.1021/acs.jpca.4c05611. PMID: 39432261.

[32] Hays, B. M. & Widicus Weaver, S. L. Theoretical examination of o(1d) insertion reactions to form methanediol, methoxymethanol, and aminomethanol. *The Journal of Physical Chemistry A* **117**, 7142–7148 (2013). URL https://doi.org/10.1021/jp400753r. PMID: 23646865.

[33] Lamberts, T., Fedoseev, G., Kästner, J., Ioppolo, S. & Linnartz, H. Importance of tunneling in h-abstraction reactions by oh radicals-the case of ch4+ oh studied through isotope-substituted analogs. *Astronomy & Astrophysics* **599**, A132 (2017).

[34] NIST Mass Spectrometry Data Center. Pentanal (2025). URL https://webbook.nist.gov/cgi/cbook.cgi?ID=C110623&Mask=200#Mass-Spec.

[35] NIST Mass Spectrometry Data Center. Pentanoic acid (2025). URL https://webbook.nist.gov/cgi/cbook.cgi?ID=C109524&Mask=200#Mass-Spec.

[36] Jing, D. *et al.* On Water Formation in the Interstellar Medium: Laboratory Study of the O+D Reaction on Surfaces. *apjl* **741**, L9 (2011).

[37] Noble, J. A., Cuppen, H. M., Coussan, S., Redlich, B. & Ioppolo, S. Infrared resonant vibrationally induced restructuring of amorphous solid water. *The Journal of Physical Chemistry C* **124**, 20864–20873 (2020). URL https://doi.org/10.1021/acs.jpcc.0c04463.

[38] Manna, A., Pal, S., Sinha, S. & Mondal, S. K. Organic acid chemistry in ism: Detection of formic acid and its prebiotic chemistry in hot core g358.93 0.03 mm1. *Research in Astronomy and Astrophysics* **26**, 035019 (2026). URL https://doi.org/10.1088/1674-4527/ae2f4b.

[39] Kleimeier, N. F., Eckhardt, A. K. & Kaiser, R. I. A mechanistic study on the formation of acetic acid (ch3cooh) in polar interstellar analog ices exploiting photoionization reflectron time-of-flight mass spectrometry. *The Astrophysical Journal* **901**, 84 (2020). URL https://doi.org/10.3847/1538-4357/abafa4.

[40] Cruz-Diaz, G. A., Martín-Doménech, R., Moreno, E., Muñoz Caro, G. M. & Chen, Y.-J. New measurements on water ice photodesorption and product formation under ultraviolet irradiation. *mnras* **474**, 3080–3089 (2018).

[41] Mejía, C., de Barros, A. L. F., Rothard, H., Boduch, P. & da Silveira, E. F. Swift heavy ions irradiation of water ice at different temperatures: hydrogen peroxide and ozone synthesis and sputtering yield. *Monthly Notices of the Royal Astronomical Society* **514**, 3789–3801 (2022). URL https://doi.org/10.1093/mnras/stac1489.

[42] Daniely, A. *et al.* Photochemical pathways in astronomical ices: A computational study of singlet oxygen reactions with hydrocarbons. *The Journal of Chemical Physics* **162** (2025).

[43] Krasnokutski, S. A. *et al.* Formation of extraterrestrial peptides and their derivatives. *Science Advances* **10**, eadj7179 (2024). URL https://www.science.org/doi/abs/10.1126/sciadv.adj7179.

[44] Tschersich, K. G. Intensity of a source of atomic hydrogen based on a hot capillary. *Journal of Applied Physics* **87**, 2565–2573 (2000). URL https://doi.org/10.1063/1.372220.

[45] Becke, A. D. Density-functional thermochemistry. iii. the role of exact exchange. *The Journal of Chemical Physics* **98**, 5648–5652 (1993). URL https://doi.org/10.1063/1.464913.

[46] Lee, C., Yang, W. & Parr, R. G. Development of the colle-salvetti correlation-energy formula into a functional of the electron density. *Physical review B* **37**, 785 (1988).

[47] Uc, V. H., Alvarez-Idaboy, J. R., Galano, A., García-Cruz, I. & Vivier-Bunge, A. Theoretical determination of the rate constant for oh hydrogen abstraction from toluene. *The Journal of Physical Chemistry A* **110**, 10155–10162 (2006).

[48] Li, Q. S., Zhang, Y. & Zhang, S. Direct ab initio dynamics studies of the hydrogen abstraction reactions of hydrogen atom with n-propyl radical and isopropyl radical. *Journal of Molecular Modeling* **11**, 41–47 (2005).

[49] Lin, R.-J., Wu, C.-C., Jang, S. & Li, F.-Y. Variation of reaction dynamics for oh hydrogen abstraction from glycine between ab initio levels of theory. *Journal of molecular modeling* **16**, 175–182 (2010).

[50] Truong, T. N. & Duncan, W. A new direct ab initio dynamics method for calculating thermal rate constants from density functional theory. *The Journal of chemical physics* **101**, 7408–7414 (1994).

[51] Duncan, W. T. & Truong, T. N. Thermal and vibrational-state selected rates of the ch4+ cl hcl+ ch3 reaction. *The Journal of chemical physics* **103**, 9642–9652 (1995).

[52] Caldeweyher, E., Bannwarth, C. & Grimme, S. Extension of the d3 dispersion coefficient model. *The Journal of chemical physics* **147** (2017).

[53] Hjorth Larsen, A. *et al.* The atomic simulation environment—a python library for working with atoms. *Journal of Physics: Condensed Matter* **29**, 273002 (2017).

[54] Smidstrup, S., Pedersen, A., Stokbro, K. & Jónsson, H. Improved initial guess for minimum energy path calculations. *The Journal of chemical physics* **140** (2014).

[55] Neese, F. The orca program system. *Wiley Interdiscip. Rev. Comput. Mol. Sci.* **2**, 73–78 (2012).

[56] Leonori, F. *et al.* Experimental and theoretical studies on the dynamics of the o (3p)+ propene reaction: primary products, branching ratios, and role of intersystem crossing. *The Journal of Physical Chemistry C* **119**, 14632–14652 (2015).

Supplementary Files

This is a list of supplementary files associated with this preprint. Click to download.

- SupplementaryAgeneralnonenergeticformationroutetocarboxylicandfattyacidsintheinterstellarmedium.pdf